Structural, Elastic and Optoelectronic Properties of inorganic cubic $FrBX_3$ (B = Ge, Sn; X = Cl, Br, I) perovskite: the Density Functional Theory Approach

N. Hasan[a], A. Kabir [b,*] and M. Arifuzzaman[c,*]

[a]Department of Electrical and Computer Engineering, North South University, Dhaka 1229, Bangladesh.
[b]Department of Physics, Dhaka University, Dhaka 1000, Bangladesh.
[c]Department of Mathematics and Physics, North South University, Dhaka 1229, Bangladesh.

*Corresponding author: alamgir.kabir@du.ac.bd (A. Kabir)
md.arifuzzaman01@northsouth.edu (M. Arifuzzaman)

1. Theoretical Methodology

To study the unpurposive potentiality yet of the FrBX3(B=Ge,Sn;X=Br,Cl,I), *ab initio* density functional theory (DFT) simulations based on plane wave pseudopotential approach are redacted in the CASTEP (Cambridge Serial Total Energy Package) code of Materials Studio-7.0 and Vienna *ab initio* Simulation Package (VASP).[1]–[6] Constructed unit cells in cubic for these metal halide perovskites are shown in figure 1, those are considered for the further calculations in this study. Geometry optimizations are performed with the generalized gradient approximation (GGA) for exchange correlation interactions into the Perdew-Burke-Ernzerhof (PBE) functional.[7], [8] The electron-ion interaction has been studied using the Vanderbilt model's ultrasoft pseudopotential [9] with Koelling-Harmon relativistic treatment. The Broyden-Fletcher-Goldfarb-Shanno (BFGS) algorithm [10] was used to ensure optimized crystal structure in the way of minimizing the total energy, internal forces, and stresses. In these calculations, the wave function is expanded up to 450 eV as the cutoff energy for plane wave function. The k-point sampling of the Brillouin Zone was implemented utilizing the Monkhorst-Pack scheme [11] with 10×10×10 k-points to secure better convergence. Elastic stiffness constants (C_{ij}) in this study were evaluated by employing finite strain theory within the CASTEP code [12], [13], where Voigt-Reuss-Hill (VRH) averaging scheme [13] was employed as well as the relevant equations [14], [15] that are used to calculate polycrystalline mechanical parameters. The maximum strain amplitude was set as 0.003. The optical properties are calculated and analyzed without the scissor operator regarding a clear depiction using CASTEP based DFT Kohn-Sham orbitals and supported formulae are provided in the literature. [16] In this study, the optimization threshold for geometry of the unit cell and atomic relaxation were set up in CASTEP as follows: total energy 5×10^{-6} eV/atom; maximum force 0.01 eV/Å; maximum stress 0.02 GPa and maximum displacements 5×10^{-4} Å.

2. Structural unit-cell analysis:

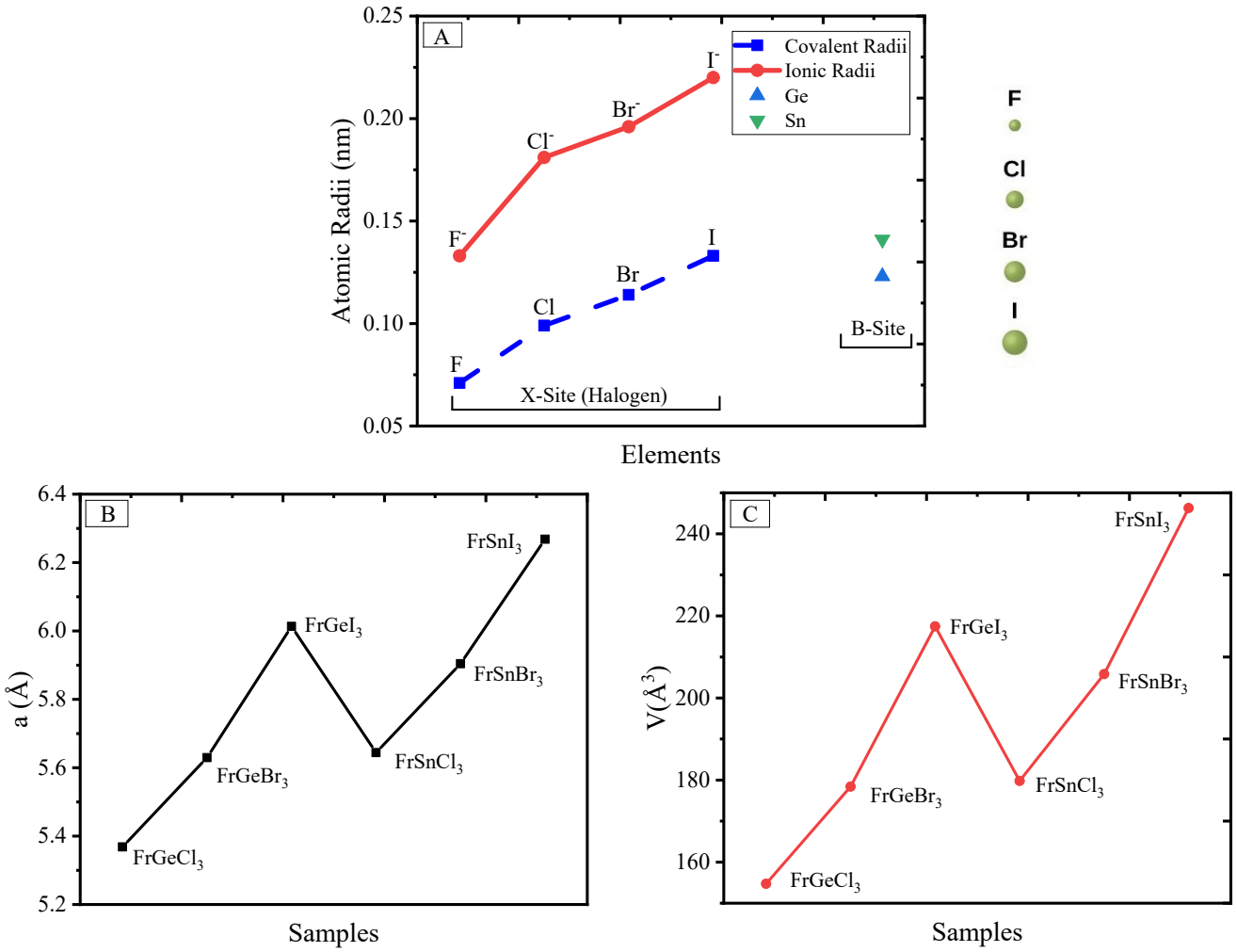

Figure S1. (A) Ionic and Covalent Radii of Halogen atoms (F, Cl, Br, I) sitting over X-site in ABX3 structure. (B) Lattice parameter (a=b=c) for FrBX3 materials (B=Ge, Sn; X=Cl, Br, I). (C) Volume of the unit cell of the studied materials.

The lattice parameters and cell volume for the cubic perovskite materials FrBX3 (B= Ge, Sn; X= Cl, Br, I) exhibit periodical behavior with changing atomic contents in B and X-sites. Figure S1(A) represent the ionic and covalent radii of the halogen atoms, the Ge atom and the Sn atom in angstrom.. The lattice parameter and cell volume increase with the replacement of halogen atom with the larger radii in the X-site as represented in Figure S1(B) & S1(C). As the ionic radii of Sn atom is larger than that of the Ge atom, the lattice parameter of the $FrSnCl_3$ is larger than that of $FrGeCl_3$, and so on as shown in the Figure S1(B) & S1(C).

3. Density of states analysis:

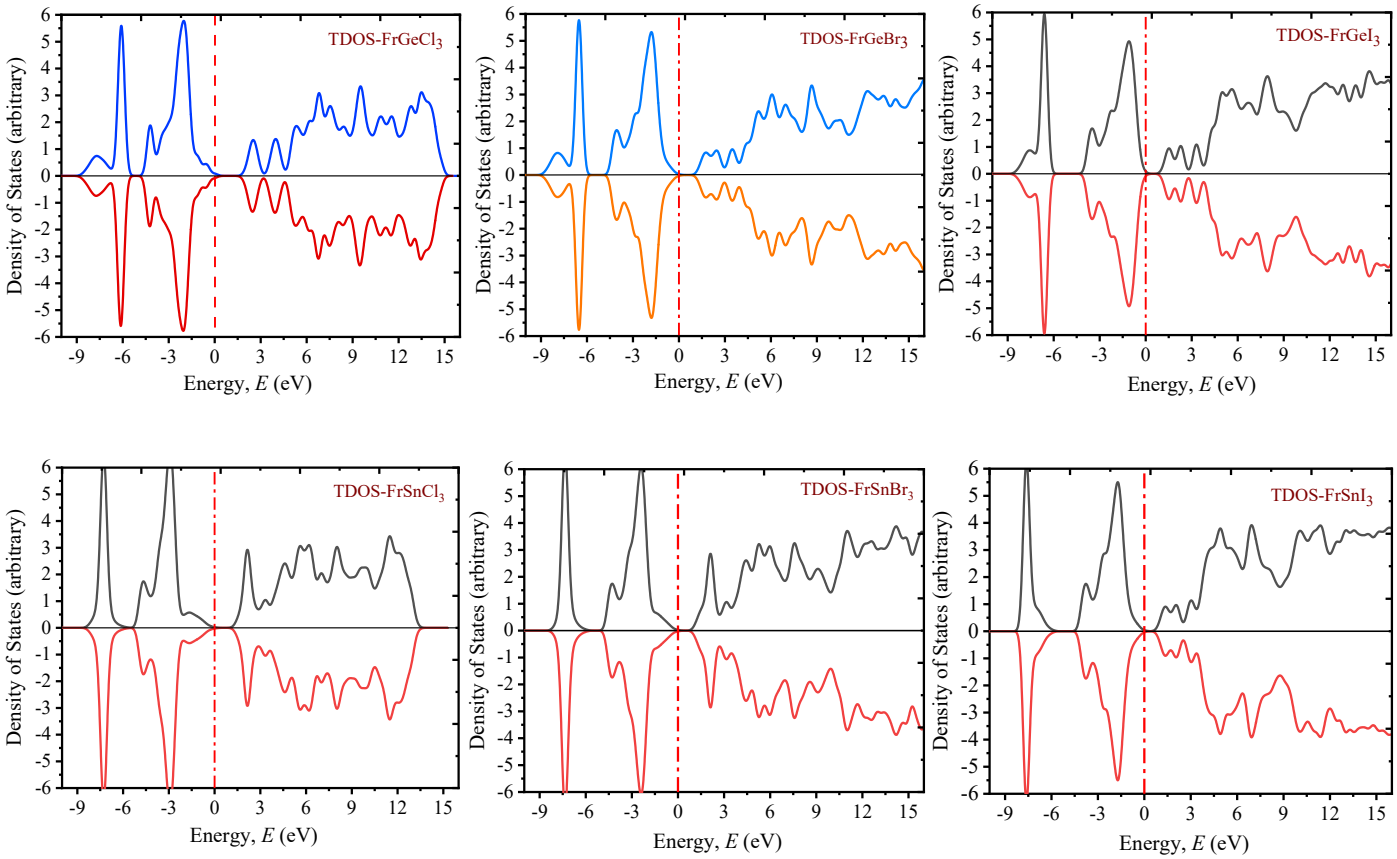

Figure S2. Total Density of States (DOS) for the investigated $FrBX_3$ (B=Ge, Sn; X=Cl, Br, I) perovskites.

3.A. Total Density of States (TDOS)

The total DOS of the six perovskite structures are presented in the Figure S2. It is clear from the figure that for all the structures the up spin and down spin contribute equally, which means the $FrBX_3$ (B=Ge, Sn; X=Cl, Br, I)) is non-magnetic in nature. The Fermi level (represent by the vertical broken red line) is just on top of the conduction band for all the six cases. It is clear from the Figure S2 that among all $FrGeX_3$, $FrGeI_3$ have the smallest bandgap, $FrGeCl_3$ have largest bandgap and $FrGeBr_3$ has the bandgap in between. The same trends is followed for the case of Sn in B sites. The electronic contribution at Fermi level is largest for the case of I in the X sites for both Ge and Sn in the B sites.

3.B. Partial Density of States (PDOS) and orbital contribution

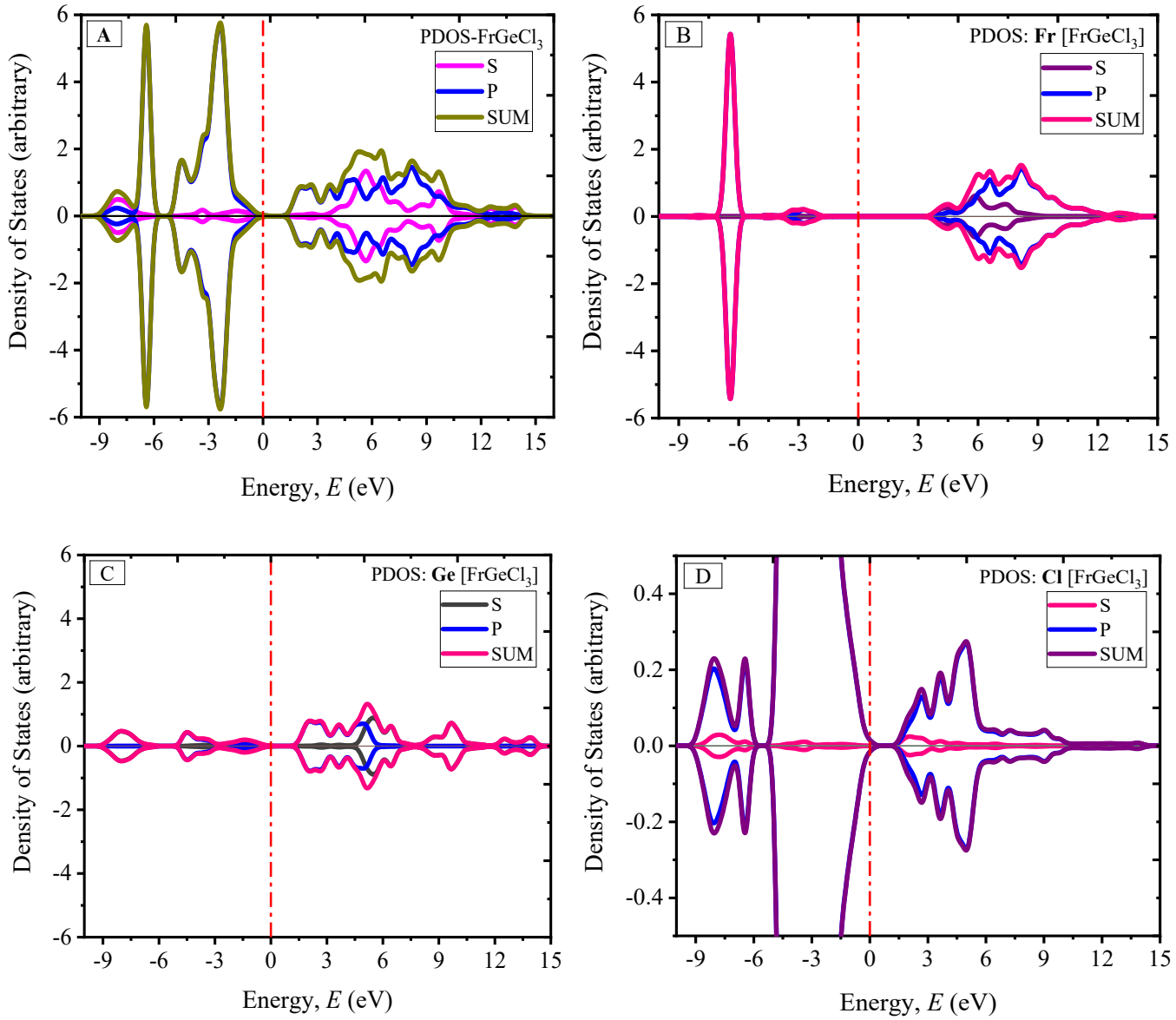

Figure S3. (A) The orbital projected DOS for $FrGeCl_3$, (B) the orbital projected DOS for Fr atom in $FrGeCl_3$, (C) the orbital projected DOS of Ge atom in $FrGeCl_3$ and (D) the orbital projected DOS for Cl atom in FrGeCl3.

The partial density of states (PDOS) of the $FrGeCl_3$ and its each element are shown in Figure S3 where the fermi energy E_F is set at 0 eV. It is clear from the Figure S3(A) that the valance band maxima and conduction band minima of the FrGeCl3 is comprised of the P-orbital, S-orbital is dominant in the deep energy level. The Fr and Ge atom's P-orbital does not have any contribution at near the Fermi level as represented in the Figure S3(B & C). The contribution from the P-orbital of the Cl atom is dominant at the conduction band minima and the valance band maxima as it is clear from the Figure S3(D).

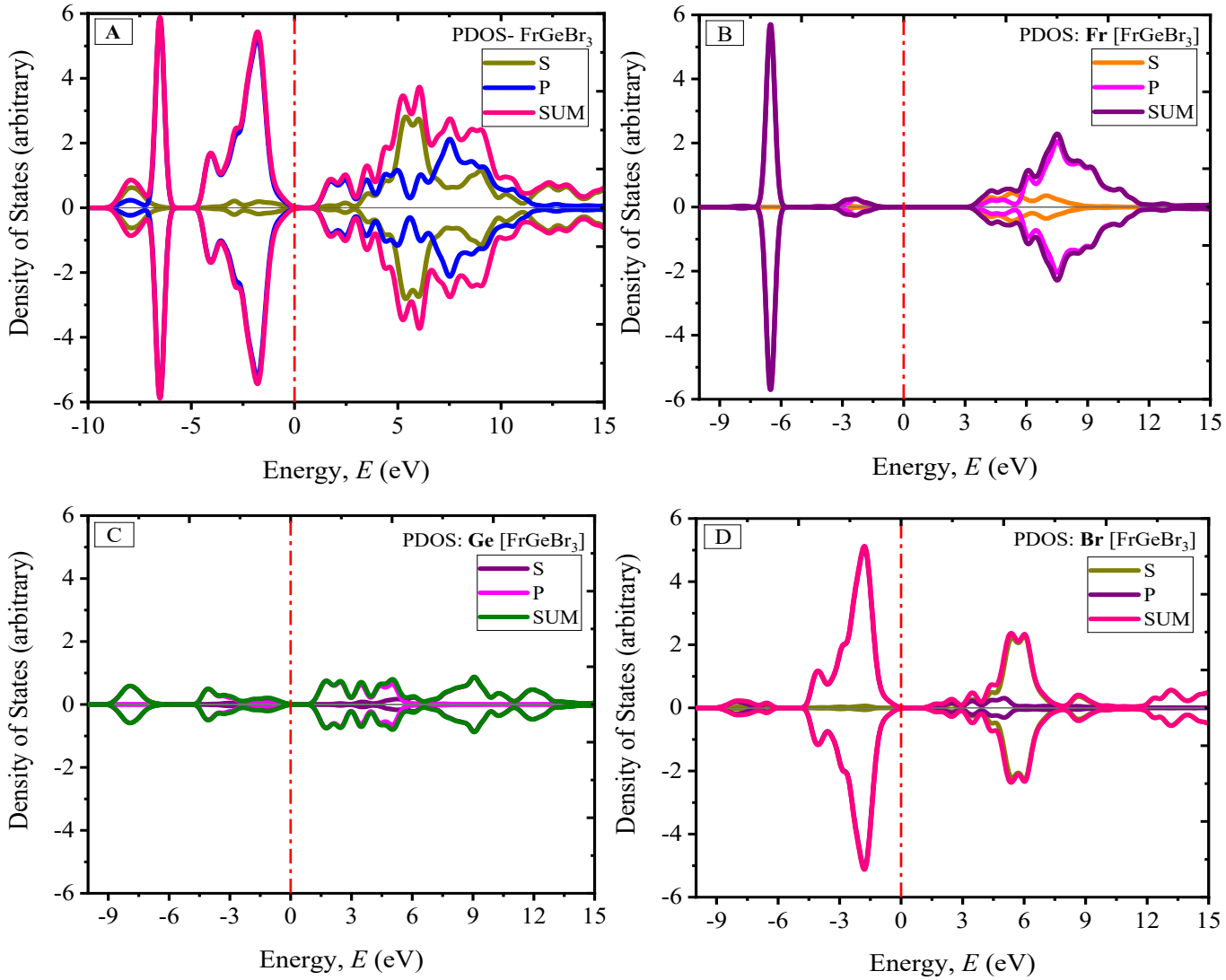

Figure S4. Partial Density of States (PDOS) for $FrGeBr_3$ (A) and its Fr (B), Ge (C), Br (D) elements.

Figure S4 depicts the partial density of states (PDOS) of $FrGeBr_3$ and its constituent elements with the fermi energy set to 0 eV. Figure S4(A), S4(B), S4(C), and S4(D) show that the contribution from the P orbital is greater than that of the S orbital around the fermi energy level in all cases (D). Whereas Cl's p orbital contributed primarily below the fermi energy level, besides Br's S orbital, and Fr and Ge's p orbital contributed primarily above the fermi energy level.

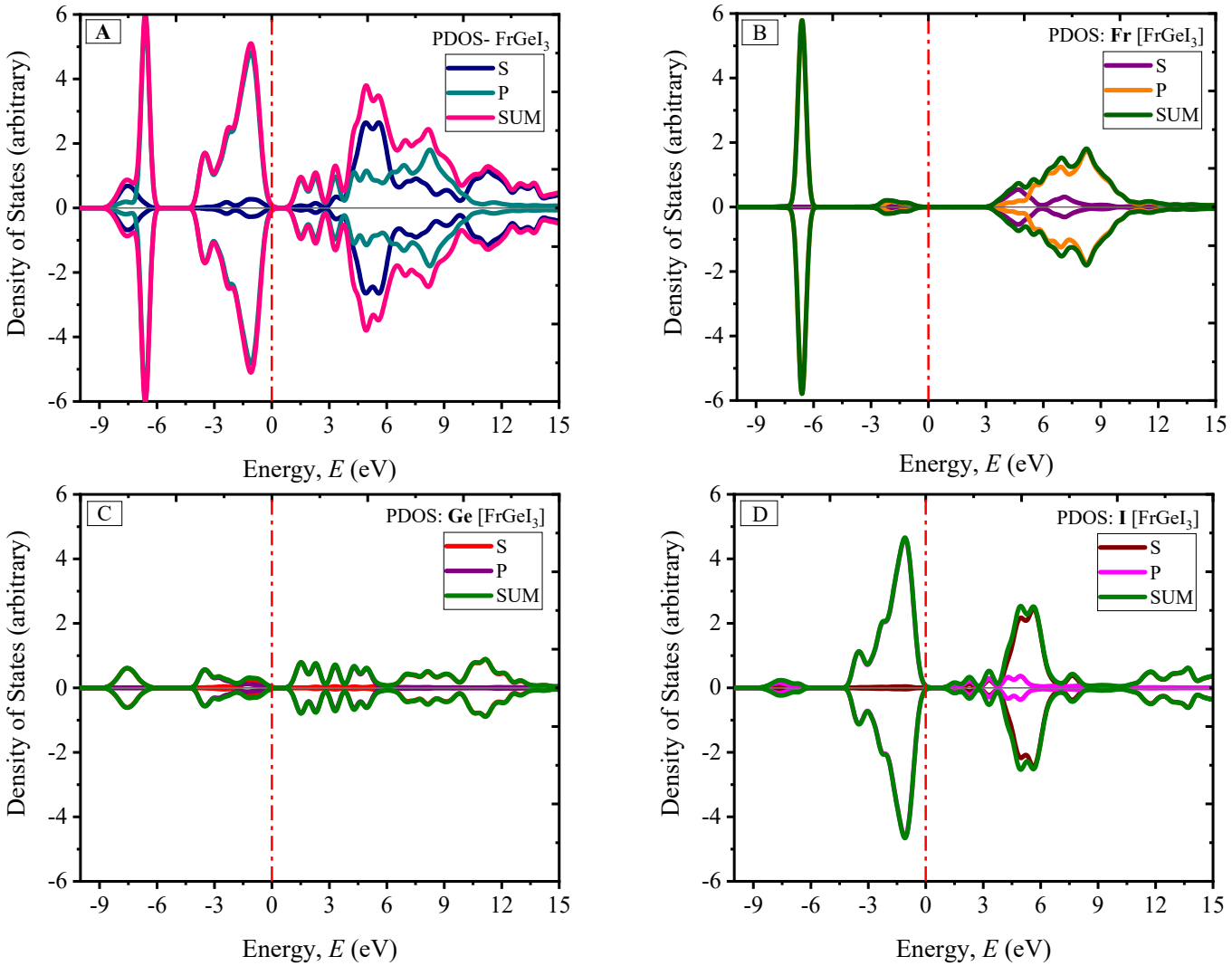

Figure S5. Partial Density of States (PDOS) for $FrGeI_3$ (A) and its Fr (B), Ge (C), I (D) elements.

Figure S5 depicts the partial density of states (PDOS) of FrGeI3 and its individual elements, with the fermi energy E_F set to 0 eV. In all cases, as seen in Figure S5(A), S5(B), S5(C), and S5(D), the P orbital contributes more to the fermi energy level than the S orbital in all circumstances. The contribution of I's p orbital was primarily below the fermi energy level, while the contribution of the p orbital of A site atom Fr and B site atom Ge was primarily above the fermi energy level.

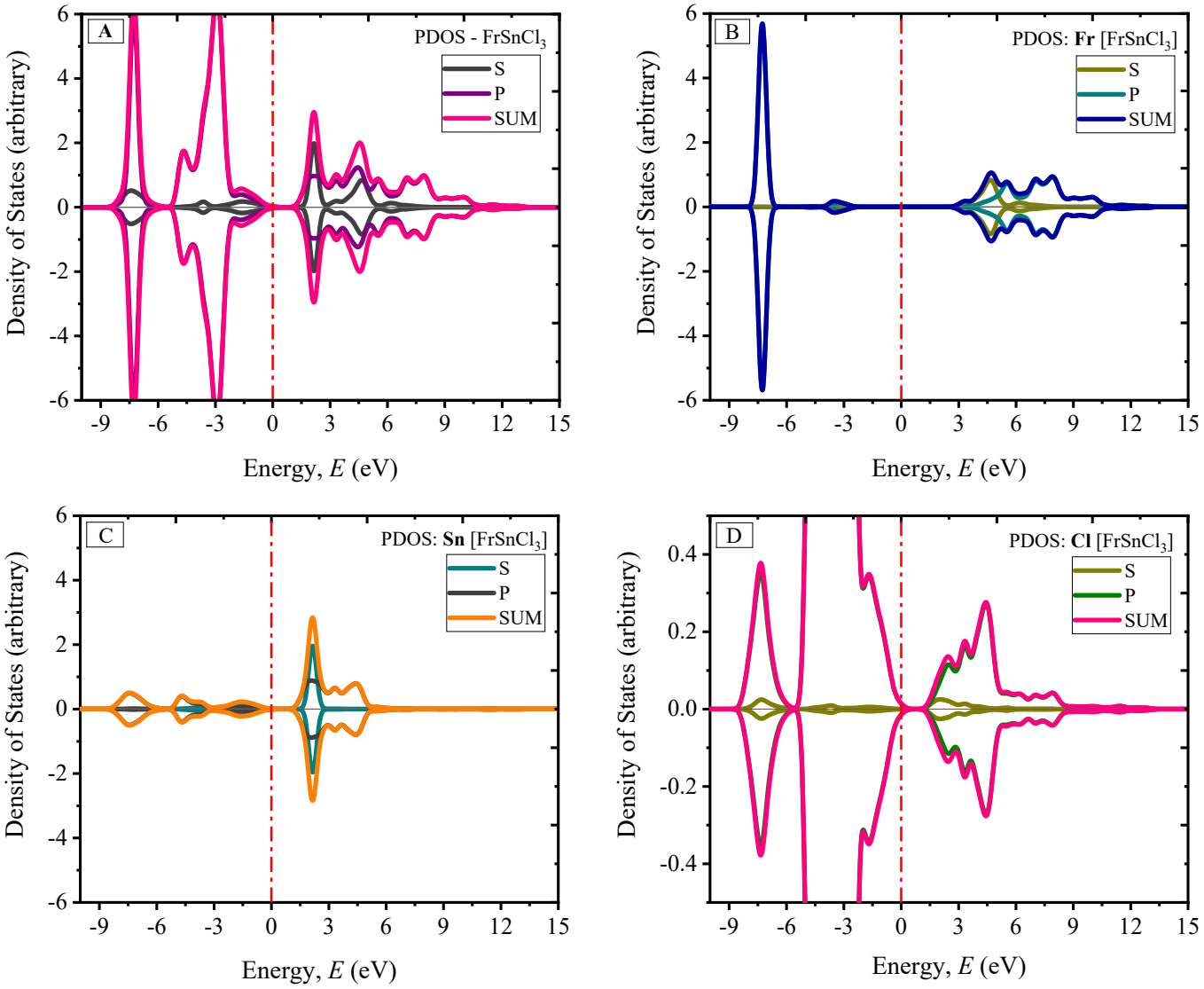

Figure S6. Partial Density of States (PDOS) for $FrSnCl_3$ (A) and its Fr (B), Sn (C), Cl (D) elements.

With the fermi energy E_F set to 0 eV, Figure S6 illustrates the partial density of states (PDOS) of $FrSnCl_3$ and its constituent elements. The P orbital contributes more to the fermi energy level than the S orbital in all cases, as shown in Figure S6(A), S6(B), S6(C), and S6(D). Cl's p orbital contributed predominantly below the fermi energy level, whereas the s and p orbitals of A site atom Fr and B site atom Sn contributed primarily above the fermi energy level.

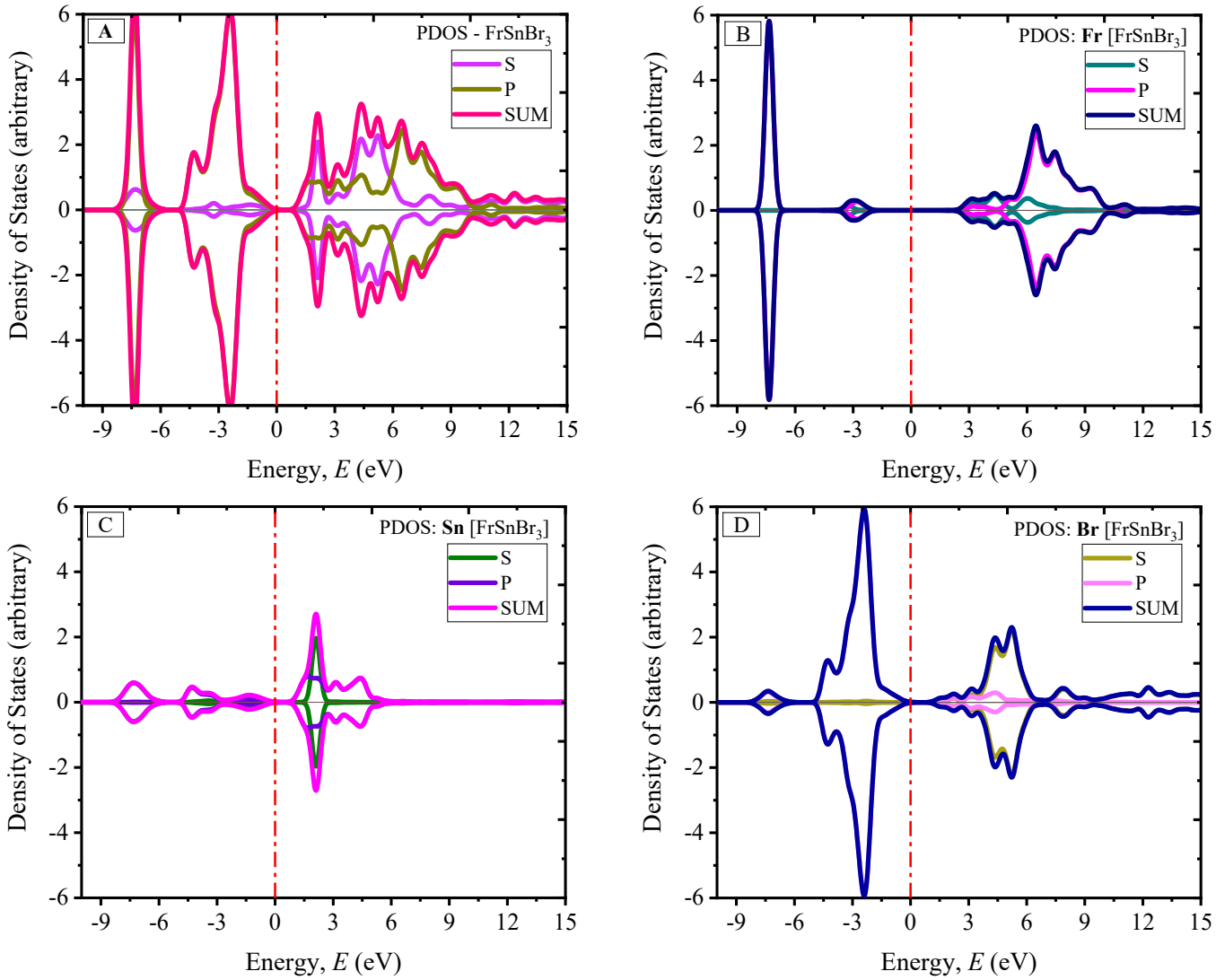

Figure S7. Partial Density of States (PDOS) for $FrSnBr_3$ (A) and its Fr (B), Sn (C), Br (D) elements.

Figure S7 demonstrates the partial density of states (PDOS) of $FrSnBr_3$ and its individual elements, with the fermi energy E_F set to 0 eV. The S and P orbital contributes to the fermi energy level's electronic density of states in all conditions, as shown in Figure S7(A), S7(B), S7(C), and S7(D). The p orbital of Br contributed predominantly below the fermi energy level, whereas the p orbital of A site atom Fr and s orbital of B site atom Sn contributed primarily above the fermi energy level.

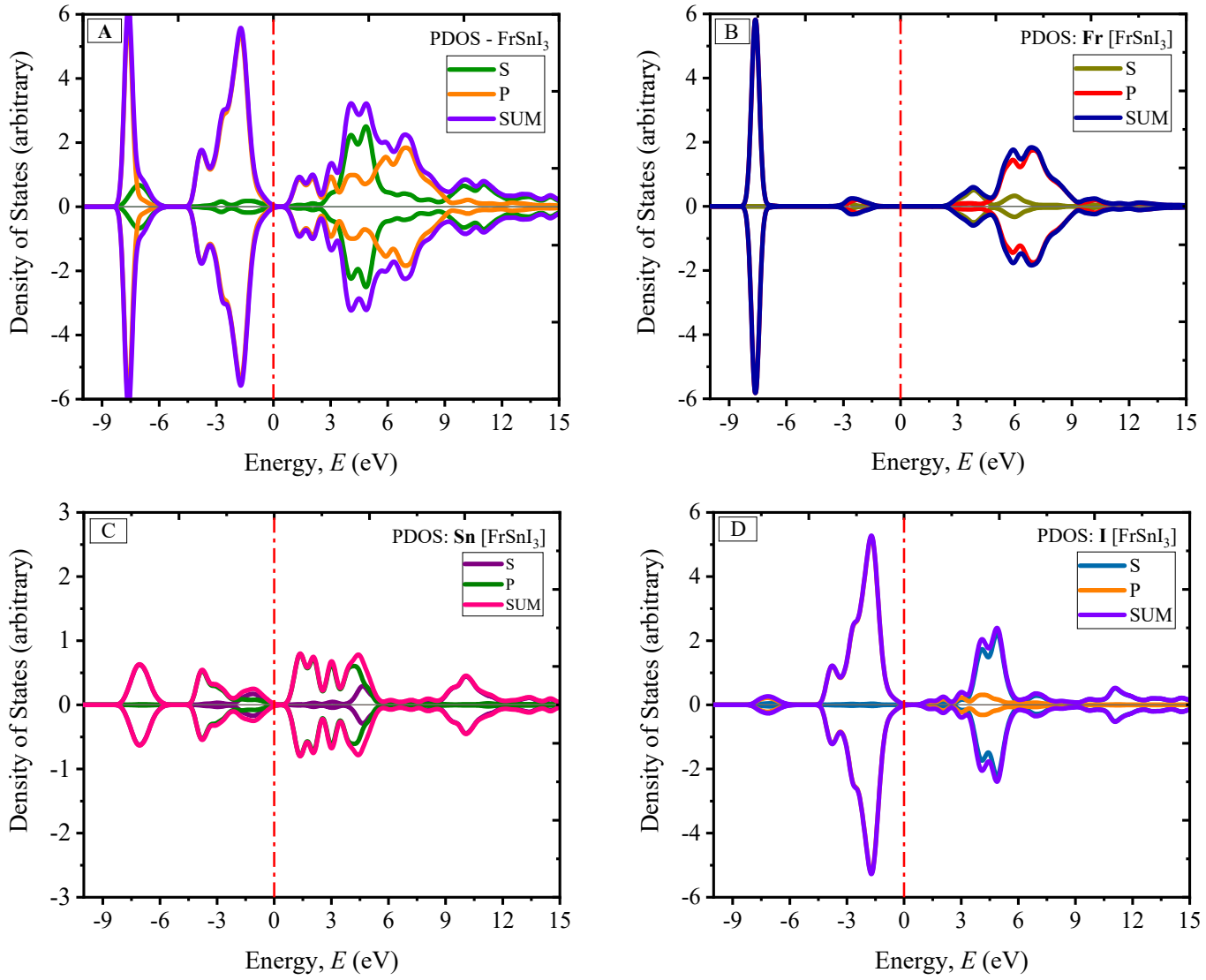

Figure S8. Partial Density of States (PDOS) for FrSnI3 (A) and its Fr (B), Sn (C), I (D) elements.

With the fermi energy E_F set to 0 eV, Figure S8 presents the partial density of states (PDOS) of $FrSnI_3$ and its constituent elements. Figure S8(A), S8(B), S8(C), and S8(D) show how the S and P orbitals contribute to the electronic density of states of the Fermi energy level in all situations. Br's p orbital contributed mostly below the Fermi energy level, whilst A site atom Fr's p orbital and B site atom Sn's p orbital contributed primarily above the Fermi energy level.

4. Optical refraction

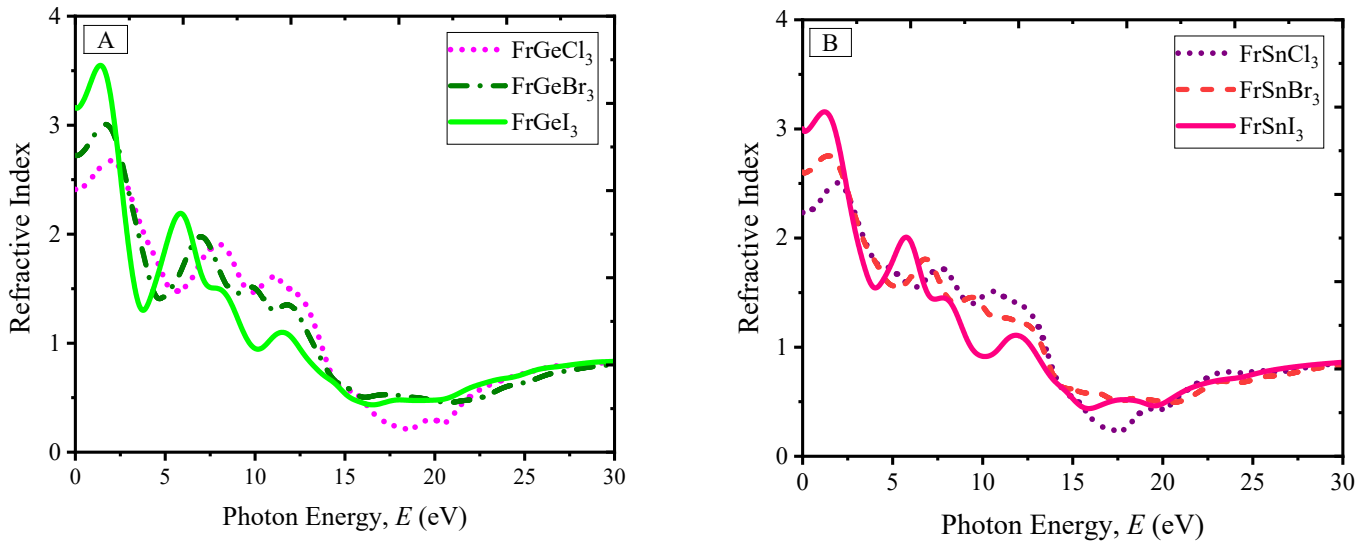

Figure S9. Refractive Index as a function of photon's energy for $FrGeX_3$ (A) and $FrSnX_3$ (B) perovskites.

Figure S9 represent the refractive index of the studied series of $FrBX_3$ (B= Ge, SN; X=Cl, Br, I) perovskites as a function of photon's energy up to the energy of 30 eV. For both the Ge and Sn content in the B sites the perovskite follow almost the same trends in the refractive index, except the peak value is larger for the case of Ge in B sites than Sn in B sites. As compared among the halogens, I atom in the X sites give the maximum value of refractive index for both the Ge and Sn case. The peak value is for approximately 2 eV of photon energy for both the cases.

5. PCE

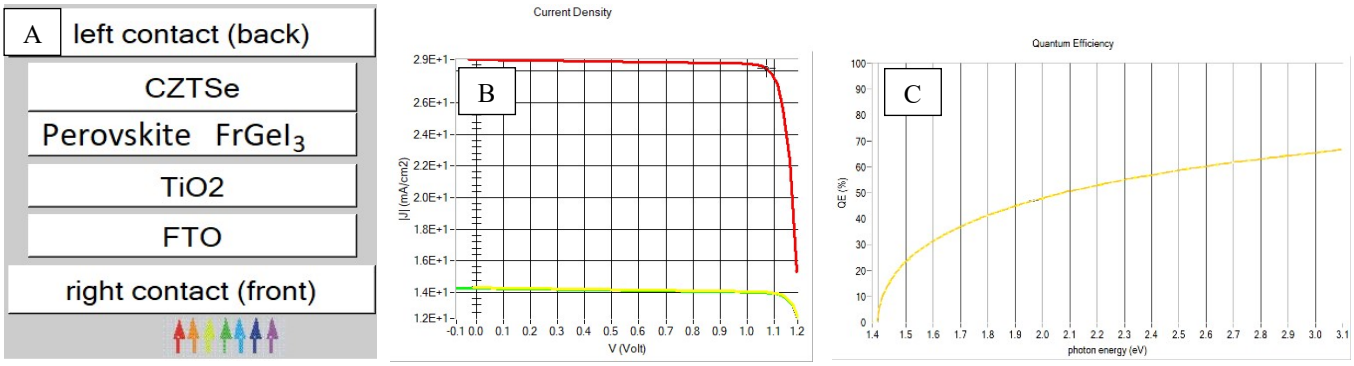

Figure S10. Simulated solar cell power conversion efficiency (PCE) for $FrGeI_3$ perovskite material (A) the solar cell device structure, (B) I-V curve and (C) QE curve.

The I-V curve extracted open circuit voltage is found as Voc= 1.4870V, and the current density Jsc=14.312 mA/cm^2 and the fill factor FF=73.75%. Employing these values, the PCE was evaluated using the following relation, $\eta = \frac{\beta_{FF} * V_{OC} * J_{SC}}{P_{solar}}$ and the PCE values is found to be 15.70%. The optimization in setting the parameters for the layer materials in defining the solar cell device with Fr containing perovskite is necessary for further investigations. The extracted quantum efficiency (QE) shows at the range of 2-3 eV photon energy it follows to increase and found about highest 65% of QE.

References:

[1] W. Kohn and L. J. Sham, "Self-Consistent Equations Including Exchange and Correlation Effects," *Physical Review*, vol. 140, no. 4A, Nov. 1965, doi: 10.1103/PhysRev.140.A1133.

[2] P. Hohenberg and W. Kohn, "Inhomogeneous Electron Gas," *Physical Review*, vol. 136, no. 3B, Nov. 1964, doi: 10.1103/PhysRev.136.B864.

[3] S. J. Clark *et al.*, "First principles methods using CASTEP," *Zeitschrift für Kristallographie - Crystalline Materials*, vol. 220, no. 5–6, May 2005, doi: 10.1524/zkri.220.5.567.65075.

[4] M. D. Segall *et al.*, "First-principles simulation: ideas, illustrations and the CASTEP code," *Journal of Physics: Condensed Matter*, vol. 14, no. 11, Mar. 2002, doi: 10.1088/0953-8984/14/11/301.

[5] M. C. Payne, M. P. Teter, D. C. Allan, T. A. Arias, and J. D. Joannopoulos, "Iterative minimization techniques for *ab initio* total-energy calculations: molecular dynamics and conjugate gradients," *Reviews of Modern Physics*, vol. 64, no. 4, Oct. 1992, doi: 10.1103/RevModPhys.64.1045.

[6] G. Kresse and J. Furthmüller, "Efficiency of ab-initio total energy calculations for metals and semiconductors using a plane-wave basis set," *Computational Materials Science*, vol. 6, no. 1, Jul. 1996, doi: 10.1016/0927-0256(96)00008-0.

[7] J. P. Perdew, K. Burke, and M. Ernzerhof, "Generalized Gradient Approximation Made Simple," *Physical Review Letters*, vol. 77, no. 18, Oct. 1996, doi: 10.1103/PhysRevLett.77.3865.

[8] J. Paier, R. Hirschl, M. Marsman, and G. Kresse, "The Perdew–Burke–Ernzerhof exchange-correlation functional applied to the G2-1 test set using a plane-wave basis set," *The Journal of Chemical Physics*, vol. 122, no. 23, Jun. 2005, doi: 10.1063/1.1926272.

[9] D. Vanderbilt, "Soft self-consistent pseudopotentials in a generalized eigenvalue formalism," *Physical Review B*, vol. 41, no. 11, Apr. 1990, doi: 10.1103/PhysRevB.41.7892.

[10] T. H. Fischer and J. Almlof, "General methods for geometry and wave function optimization," *The Journal of Physical Chemistry*, vol. 96, no. 24, Nov. 1992, doi: 10.1021/j100203a036.

[11] H. J. Monkhorst and J. D. Pack, "Special points for Brillouin-zone integrations," *Physical Review B*, vol. 13, no. 12, Jun. 1976, doi: 10.1103/PhysRevB.13.5188.

[12] F. D. Murnaghan, "Finite Deformations of an Elastic Solid," *American Journal of Mathematics*, vol. 59, no. 2, Apr. 1937, doi: 10.2307/2371405.

[13] R. Hill, "The Elastic Behaviour of a Crystalline Aggregate," *Proceedings of the Physical Society. Section A*, vol. 65, no. 5, May 1952, doi: 10.1088/0370-1298/65/5/307.

[14] J. Islam and A. K. M. A. Hossain, "Narrowing band gap and enhanced visible-light absorption of metal-doped non-toxic $CsSnCl_3$ metal halides for potential optoelectronic applications," *RSC Advances*, vol. 10, no. 13, 2020, doi: 10.1039/C9RA10407K.

[15] Md. Z. Rahaman, Md. A. Rahman, and Md. A. R. Sarker, "Prediction of a new transition metal oxide $MgRhO_3$ with $SrTiO_3$-type structure: Stability, structure and physical characteristics," *Chinese Journal of Physics*, vol. 55, no. 4, Aug. 2017, doi: 10.1016/j.cjph.2017.03.021.

[16] M. A. Hadi, R. v. Vovk, and A. Chroneos, "Physical properties of the recently discovered $Zr2(Al_{1-x}Bi_x)C$ MAX phases," *Journal of Materials Science: Materials in Electronics*, vol. 27, no. 11, Nov. 2016, doi: 10.1007/s10854-016-5338-z.